Published in final edited form as:
Nature. 2013 September 5; 501(7465): 63–68. doi:10.1038/nature12510.

Key tissue targets responsible for anthrax toxin-induced-lethality

Shihui Liu[1], **Yi Zhang**[1], **Mahtab Moayeri**[1], **Jie Liu**[2], **Devorah Crown**[1], **Rasem Fattah**[1], **Alexander N. Wein**[1], **Zu-Xi Yu**[3], **Toren Finkel**[2], and **Stephen H. Leppla**[1]

[1]Microbial Pathogenesis Section, Laboratory of Parasitic Diseases, National Institute of Allergy and Infectious Diseases, National Institutes of Health, Bethesda, MD 20892

[2]Center for Molecular Medicine, National Heart, Lung, and Blood Institute, National Institutes of Health, Bethesda, MD 20892

[3]Pathology Core Facility, National Heart, Lung, and Blood Institute, National Institutes of Health, Bethesda, MD 20892

Summary

Bacillus anthracis, the causative agent of anthrax disease, is lethal due to the actions of two exotoxins, anthrax lethal toxin (LT) and edema toxin (ET). The key tissue targets responsible for the lethal effects of these toxins are unknown. Here we generated cell-type specific anthrax toxin receptor capillary morphogenesis protein-2 (CMG2)-null mice and cell-type specific CMG2-expressing mice and challenged them with the toxins. Our results show that lethality induced by LT and ET occur through damage to distinct cell-types; while targeting cardiomyocytes and vascular smooth muscle cells is required for LT-induced mortality, ET-induced lethality occurs mainly through its action in hepatocytes. Surprisingly, and in contradiction to what has been previously postulated, targeting of endothelial cells by either toxin does not appear to contribute significantly to lethality. Our findings demonstrate that *B. anthracis* has evolved to use LT and ET to induce host lethality by coordinately damaging two distinct vital systems.

Introduction

Bacillus anthracis, the causative agent of anthrax, causes disease by growing to high numbers in the blood and secreting the anthrax exotoxins, consisting of three components: protective antigen (PA), lethal factor (LF), and edema factor (EF) [1]. PA is the receptor-binding moiety that binds to either tumor endothelium marker-8 (TEM8, or anthrax toxin

For correspondence: Shihui Liu: shliu@niaid.nih.gov, Stephen H. Leppla: sleppla@niaid.nih.gov.

Author Contributions

Y.Z. maintained mouse colonies and performed animal experiments. M.M. and J.L. designed, performed experiments, analyzed data, and edited the paper. D.C. performed animal experiments. R.F. purified proteins. A.N.W. made the CMG2 transgenic construct. Z.X. performed histological analyses. T.F. was involved in scientific discussions, providing reagents, and edited the paper. S.H.L. supervised research and edited the paper. S.L. conceived and supervised the project, designed and performed experiments, analyzed data, and wrote the paper.

The authors declare no competing financial interests.

Readers are welcome to comment on the online version of the paper.

receptor 1) or capillary morphogenesis protein-2 (CMG2, or anthrax toxin receptor 2) on target cells [2–4]. LF and EF then bind to receptor-associated PA and are transported to the cytosol. The *in vivo* toxic effects of LT and ET are principally mediated through PA binding to CMG2 [4]. EF, which with PA forms edema toxin (ET), is a calmodulin-dependent adenylate cyclase that elevates intracellular cAMP levels and has been shown to cause skin edema and lethality in experimental animals [5,6]. LF, which forms lethal toxin (LT) with PA, is lethal to animals. LF is a Zn^{+2}-dependent metalloproteinase that cleaves and inactivates the mitogen-activated protein kinase kinases [7–9] and inflammasome sensor Nlrp1 [10,11].

The toxins play essential roles in anthrax pathogenesis [12]. At the early stages of infection, LT and ET coordinately impair the immune system to establish infection [13,14]. At later stages, the toxins accumulate to high levels and cause death through mechanisms that are still not fully understood, despite studies in challenge models ranging from zebra fish to non-human primates [14–18]. The consequences of targeting specific tissues or cell-types cannot be accurately assessed in systemic challenge models. In this study we generated various cell-type specific CMG2-null mice as well as the corresponding cell-type specific CMG2-expressing mice, and identified the key tissue targets of LT and ET.

Results

LT targeting of endothelial is not lethal to mice

Anthrax toxins induce a vascular shock state in animal models [15], and this has been hypothesized to be due to their effects on the endothelium [14,17–21]. To assess the role of endothelial cells (ECs), we generated EC-specific CMG2-null mice (*CMG2(EC)*$^{-/-}$) (Table 1 and Extended Data Fig. 1a, 1b) in which the EC-specific deletion of CMG2 was verified. ECs isolated from the lungs of *CMG2(EC)*$^{-/-}$ mice were 300-fold more resistant than ECs from control CMG2$^{f/f}$ mice to FP59 [22,23], a LF fusion toxin that kills cell in a PA-dependent manner (Extended Data Fig. 1c). *CMG2(EC)*$^{-/-}$ ECs also became resistant to proliferation arrest induced by LT (Extended Data Fig. 1d). Interestingly, *CMG2(EC)*$^{-/-}$ ECs were completely resistant to a PA mutant (PA-L687A) that binds preferentially to CMG2 over TEM8 (Extended Data Fig. 1e, 1f), further confirming the complete deletion of CMG2 in *CMG2(EC)*$^{-/-}$ ECs. In contrast, the cells other than ECs (non-ECs) from both *CMG2(EC)*$^{-/-}$ and control *CMG2*$^{f/f}$ mice were similarly sensitive to both PA variants (Extended Data Fig. 1c, 1f). Thus, CMG2, the major anthrax toxin receptor in ECs, was specifically and completely deleted from ECs in *CMG2(EC)*$^{-/-}$ mice.

To determine the role of targeting ECs in LT pathogenesis *in vivo*, we challenged the *CMG2(EC)*$^{-/-}$ mice with 100 μg LT. Surprisingly, the *CMG2(EC)*$^{-/-}$ mice displayed similar sensitivity as their *CMG2(EC)*$^{+/-}$ and *CMG2*$^{+/+}$ littermates in a manner independent of challenge route while whole-body *CMG2*$^{-/-}$ mice were completely resistant (Fig. 1a and Extended Data Fig. 1g, 1h). Therefore, LT targeting of ECs appears to not be required for lethality.

To examine the possibility that damaging ECs alone would induce symptoms or lethality, we also generated CMG2 transgenic mice in which CMG2 was expressed only in ECs. The CMG2 transgenic vector contains a loxP-stop-loxP (LSL) cassette[24] with an EGFP coding

sequence located between the ubiquitous CAG promoter and the CMG2 transgene (Extended Data Fig. 2a). Thus, the resulting transgenic mice (*LSL-CMG2*) exhibited whole body green fluorescence and did not express the transgene until bred with tissue-specific *Cre*-transgenic mice, allowing loss of LSL cassette and fluorescence in particular tissue. EC-specific CMG2-expressing mice ($CMG2^{EC}$, Table 1) were obtained by breeding *LSL-CMG2* mice with *Cdh-Cre* mice, and by subsequent breeding with whole-body $CMG2^{-/-}$ mice to eliminate expression of the endogenous CMG2. We confirmed the EC-restricted expression of the CMG2 transgene by demonstrating the regained sensitivity of ECs from $CMG2^{EC}$ mice to PA + FP59 and PA-L687A + FP59 (Extended Data Fig. 2b, 2c). As expected, non-ECs from $CMG2^{EC}$ and whole-body $CMG2^{-/-}$ mice, which only expressed the minor receptor TEM8, had similar intermediate sensitivities to PA + FP59 and were fully resistant to PA-L687A + FP59 (Extended Data Fig. 2b, 2c). These results demonstrate that CMG2 transgene is specifically expressed in ECs of $CMG2^{EC}$ mice. We then challenged the $CMG2^{EC}$ mice with LT. Remarkably, all the $CMG2^{EC}$ mice survived two doses of 100 μg LT, whereas all their littermate $CMG2^{+/+}$ and $CMG2^{+/-}$ control mice succumbed to the challenges (Fig. 1b). The above results unequivocally demonstrate that LT targeting of ECs is insufficient to cause lethality *in vivo*.

LT targets cardiomyocytes and smooth muscle cells

We next examined the effects on LT pathogenesis of targeting the other two major cell-types of the cardiovascular system by generating cardiomyocyte (CM)- and vascular smooth muscle cell (SM)-specific CMG2-null mice (Table 1). The CM-specific CMG2-null mice ($CMG2(CM)^{-/-}$, Table 1) had CMG2 deleted only in heart tissue (Extended Data Fig. 3a, left panel). The $CMG2^{f/f}$/*SM22-Cre* mice showed the deletion occurred both in the aorta (enriched with vascular SMs) and the heart (Extended Data Fig. 3a, right panel), and therefore are referred to as $CMG2(SM/CM)^{-/-}$ mice (Table 1), reflecting the fact that they are actually SM/CM-specific CMG2-null mice. This is consistent with a previous study showing that the SM22α promoter is active in both SMs and CMs [25]. We found that both $CMG2(CM)^{-/-}$ and $CMG2(SM/CM)^{-/-}$ mice were more resistant than their littermate controls to LT challenge, in that 52% of the $CMG2(CM)^{-/-}$ mice and nearly all of the $CMG2(SM/CM)^{-/-}$ mice survived (Fig. 2a, 2b and Extended Data Fig. 3b). Therefore, CMs and SMs appear to be major targets for LT-induced lethality.

To further verify this finding, we further generated CM-specific ($CMG2^{CM}$, Table 1) or SM and CM-specific ($CMG2^{SM/CM}$, Table 1) CMG2-expressing mice using the strategy described for generation of $CMG2^{EC}$ mice above (Extended Data Fig. 2a and Methods section), where loss of GFP expression in CMs or CMs/SMs but not in other cell-types was verified (Fig. 2c, 2d and Extended Data Fig. 4). Interestingly, the activation of the CMG2 transgene occurred selectively in vascular SMs in aorta but not in SM layer in small intestines and uterus of the $CMG2^{SM/CM}$ mice (Fig. 2d and Extended Data Fig. 4b). Strikingly, 100% of the $CMG2^{CM}$ and $CMG2^{SM/CM}$ mice regained sensitivity and succumbed to two doses of LT (100 μg) whereas all the whole-body $CMG2^{-/-}$ and the *LSL-CMG2*/$CMG2^{-/-}$ mice survived without any sign of disease (Fig. 2e–2h). Sensitivity of the $CMG2^{SM/CM}$ mice was significantly higher than that of the $CMG2^{CM}$ mice in that 80% vs. 30% of these mice, respectively, were killed by only one dose of LT ($P = 0.05$) (Fig. 2e–2h).

These results clearly demonstrate that CMs as well as SMs are key targets of LT. Although nearly all mice with CMG2 deletion in SMs and CMs survived one dose of LT challenge (Fig. 2b and Fig. 3a), most of the mice were unable to survive two doses (Fig. 3b). This suggests that other target cells could contribute to lethality at higher doses of toxin. To evaluate whether the additional deletion of CMG2 in ECs could augment the LT resistance of *CMG2(SM/CM)*$^{-/-}$ mice, we generated the mice with CMG2 deletion in CMs, SMs, and ECs (*CMG2(SM/CM/EC)*$^{-/-}$, Table 1) and found that they were more resistant to LT than *CMG2(SM/CM)*$^{-/-}$ mice (Fig. 3a, 3b). These results demonstrate that the LT-induced lethality was largely due to targeting the three major cell-types of the cardiovascular system through the CMG2 receptor with LT targeting of ECs contributing to the disease progression only at higher doses.

Serum levels of c-Troponin-I, a cardiomyocyte-specific protein that is elevated during cardiac injury, were significantly increased in WT and *CMG2(EC)*$^{-/-}$ mice but remained low in both *CMG2(CM)*$^{-/-}$ and *CMG2(SM/CM)*$^{-/-}$ mice 48 h after LT challenge (Fig. 3c). Consistent with this, echocardiographic analyses showed that heart function was significantly compromised in LT-treated WT mice but not *CMG2(CM)*$^{-/-}$, *CMG2(SM/CM)*$^{-/-}$, and *CMG2*$^{-/-}$ mice (Fig. 3d). Histological analyses showed regions of cardiomyocyte degeneration in LT-treated WT but not *CMG2*$^{-/-}$ mice (Extended Data Fig. 5). Modest hepatocyte degeneration was also found in LT-treated WT but not *CMG2*$^{-/-}$ mice, perhaps reflecting previously reported LT-induced hypoxia- mediated liver damage (see below). No obvious abnormalities were found in the lungs, kidneys, and spleens of the LT-treated mice (data not shown).

Resistance to *B. anthracis* infection

B. anthracis normally exists in spore form in the environment and germinates to toxin-producing vegetative bacteria at 37°C in mammalian hosts. We next infected the *CMG2(SM/CM/EC)*$^{-/-}$mice with toxigenic, unencapsulated *B. anthracis* Sterne strain spores. Strikingly, all the *CMG2(SM/CM/EC)*$^{-/-}$ mice survived the spore challenge while littermate heterozygous control mice (Fig. 3e) and *CMG2(EC)*$^{-/-}$ mice (Extended Data Fig. 6) were sensitive, indicating that toxin targeting ECs alone plays little role in this infection model. *CMG2(SM/CM/EC)*$^{-/-}$ mice were also more resistant than the littermate controls to infection with pre-germinated vegetative *B. anthracis* (75% vs. 18% survival, $P < 0.006$) (Fig. 3f). Thus, CMG2 deficiency in the three major cell-types of the cardiovascular system is sufficient to confer the resistance to LT as well as to anthrax Sterne strain infection.

Liver is not a key target of LT

Early work in our laboratory showed hypoxia-mediated damage in the liver in response to LT [15]. In light of the above results which reveal that LT primarily induces lethality through targeting the cardiovascular system, any effects in the liver are likely to be secondary events. In support of this hypothesis, we found that hepatocyte-specific CMG2-null mice (*CMG2(Hep)*$^{-/-}$, Table 1) remained sensitive to LT (Extended Data Fig. 7a) while hepatocyte-specific CMG2-expressing mice (*CMG2*^{Hep}, Table 1) were completely resistant to the toxin (Extended Data Fig. 7b, 7c). These results clearly demonstrate that liver is not a key target of LT.

ET causes intestinal fluid influx and liver oedema

Edema toxin is another important anthrax toxin relevant to anthrax pathogenesis [1]. Subcutaneous injection of ET induces edema in experimental animals. To determine whether ET also causes edematous lesions in internal organs and to define its cell-type targets, we first measured the wet/dry ratios of various organs of mice injected with ET. ET caused remarkable fluid influx into intestinal lumen of WT as well as *CMG2(SM/CM/EC)*$^{-/-}$ mice, which did not occur in mice lacking CMG2 in the intestinal epithelial cells (IEs) (*CMG2(IE)* $^{-/-}$ and *CMG2(SM/CM/EC/IE)*$^{-/-}$mice, Table 1) (Fig. 4a). Additionally, ET induced much greater fluid accumulation in intestines in IE-specific CMG2-expressing mice (*CMG2*^{IE}, Table 1) compared to *CMG2*$^{-/-}$ mice (Fig. 4b). Taken together, these results demonstrate that ET targeting of IEs but not ECs and SMs is the cause of intestinal fluid accumulation.

Interestingly, ET also induced significant liver edema in WT as well as *CMG2(IE)*$^{-/-}$, *CMG2(SM/CM/EC)*$^{-/-}$, and *CMG2(SM/CM/EC/IE)*$^{-/-}$ mice, but not in *CMG2(Hep)*$^{-/-}$ mice (Fig. 4c). Furthermore, this ET-induced liver edema was not observed in *CMG2*$^{-/-}$ mice as well as *CMG2*^{EC}, *CMG2*^{IE}, or *CMG2*$^{SM/CM}$ transgenic mice, but occurred in the hepatocyte-specific CMG2-expressing *CMG2*^{Hep} mice at levels equal to and even exceeding those in *CMG2*$^{+/+}$ mice (Fig. 4d). Thus, ET induces liver edema by acting directly on hepatocytes rather than ECs and SMs. Similarly, ET-induced skin edema was also due to directly targeting cell-types other than ECs and SMs (Extended Data Fig. 8a). We did not detect wet/dry ratio increases in the heart, spleen, kidney, and lung of the ET-treated mice (Extended Data Fig. 8b–8f), suggesting that the edema induced by ET was limited to certain tissues including skin and liver and not a general result of cAMP increases in all organs. Indeed, significant decreases in wet/dry ratios of lungs from ET-treated mice were detected (Extended Data Fig. 8f), probably reflecting the general dehydration status of the ET-treated mice resulting from fluid displacement to skin, liver and other tissues.

Liver is a key target of ET-induced lethality

To define the cell-types that are responsible for ET-induced lethality, we next evaluated the sensitivities of the various cell-type specific CMG2-null mice described above to ET. Surprisingly, mice with CMG2 specific deletion in CMs or combined deletion in CMs, vascular SMs, ECs, as well as IEs (*CMG2(SM/CM/EC/IE)*$^{-/-}$) showed similar sensitivity to ET as their littermate controls (Extended Data Fig. 9). In contrast, the mice with CMG2 deletion only in hepatocytes (*CMG2(Hep)*$^{-/-}$) displayed remarkable resistance to ET, with 82% surviving challenge (Fig. 5a). Interestingly, while all the ET-treated *CMG2(Hep)*$^{-/-}$ survivors did show initial signs of malaise, these mice recovered within three days of the challenge (Fig. 5a, right panel). We further tested the sensitivities of the various cell-type specific CMG2-expressing mice to ET. Mice which expressed CMG2 only in ECs, CMs, and vascular SMs as well as the whole-body *CMG2*$^{-/-}$ mice remained resistant to ET and did not show significant signs of disease (Fig. 5b). In contrast, the *CMG2*^{Hep} mice were fully sensitive to ET (Fig. 5b). Furthermore, the liver damage biomarkers aspartate aminotransferase and alanine aminotransferase were found to be significantly higher in ET-treated *CMG2*$^{+/+}$ and *CMG2*^{Hep} mice than in *CMG2*$^{-/-}$ controls (Fig. 5c). Histological analyses readily identified necrotic areas in livers of ET-treated WT but not *CMG2*$^{-/-}$ mice

(Extended Data Fig. 5b). Only scattered degenerated cardiomyocytes were found in ET-treated WT but not *CMG2*$^{-/-}$ mice (Extended Data Fig. 5b). No obvious abnormalities were identified in the lungs, kidneys, and spleens of ET-treated mice (data not shown). Together, the above results clearly demonstrate that hepatocytes (but not ECs, CMs or SMs) are the key cell target of ET-induced lethality.

Discussion

Generation and analysis of the cell-type specific CMG2-null mice, and the corresponding cell-type specific CMG2-expressing mice, have allowed us to identify the target cell-types responsible for lethality induced by anthrax toxins. Expression of the major toxin receptor CMG2 in CMs and SMs (but not in hepatocytes) is required for LT-induced lethality, whereas CMG2 expression in hepatocytes (but not in CMs and SMs) is critical for ET-mediated lethality. Therefore, *B. anthracis* has evolved to use the two distinct exotoxins to induce lethality by coordinately damaging two vital but distinct systems - the cardiovascular system and liver, to complete the pathogen's life cycle. Surprisingly, ECs, the cells often considered a key target of LT, and hypothesized to induce this toxin's lethality [14,17–20], are not a primary target for either LT or ET.

Our studies also show that the previous hypoxia-mediated damage observed in the liver in response to LT is a secondary event not related to direct targeting of this organ by the toxin [15]. However, liver is the principal target of ET. In addition to subcutaneous edema and fluid accumulation in the intestinal lumen, ET targeting of hepatocytes induces a unique liver edema, which does not occur in other internal organs. Hepatocyte-specific CMG2-null mice were remarkably resistant to ET and, importantly, the mice with CMG2 expressed only in hepatocytes were susceptible to this toxin.

The relative importance of LT and ET in anthrax infections remains uncertain. LF and EF have been measured in the blood of infected animals. In nearly every successful measurement of toxin levels, LF concentrations exceeded those of EF. A recent analysis of *in vivo* toxin levels in anthrax-infected rabbits found LF at 10–35 μg/ml by 48 h and EF at about 5-fold lower concentrations [26]. The 5:1 ratio of LF:EF has also been found in other anthrax infection models [27 28]. Thus, it is likely that lethal doses of ET may only be achieved in the very late stages of anthrax infection and that the majority of symptoms of infected animals may be caused by LT. Consistent with this view, we observed that the LT-resistant mice created in this study are much more likely to survive anthrax infections.

The findings reported here may have value in understanding the pathogenesis of human anthrax infections. Recognition that the anthrax toxins are targeting the cardiovascular system (LT) and liver (ET) may suggest specific supportive therapies that would limit tissue damage and increase survival. Reexamination of the clinical course, pathology, and autopsy reports of the relatively few well documented human anthrax cases [29,30] in light of the data presented here may provide additional insights.

Methods

Generation of tissue-specific CMG2-null mice

The mice having the CMG2 transmembrane (TM) domain-encoding exon 12 flanked by loxP sites (a "floxed" allele), namely, the *CMG2$^{f/f}$* mice (C57BL/6 background), were described previously [4]. To generate mice having CMG2 deleted only in ECs, the *CMG2$^{f/f}$* mice were mated with *Cdh-Cre* transgenic mice [35] (Cre-recombinase under the VE-cadherin promoter) (006137, the Jackson Laboratory, Bar Harbor, Maine, USA). EC-specific CMG2-null mice (*CMG2(EC)$^{-/-}$*) were obtained by the subsequent intercrossing of the resulting *CMG2$^{+/fl}$/Cdh-Cre* mice (see Table 1 for nomenclature). Similarly, to generate mice with CMG2 deleted in CMs, SMs, hepatocytes, and IEs, the *CMG2$^{f/f}$* mice were mated with *Myh6-Cre* [36] (Cre-recombinase under CM-specific α myosin heavy polypeptide 6 promoter) (011038, the Jackson Laboratory), *SM22-Cre* [37] (Cre-recombinase under the vascular SM-specific smooth muscle protein 22α promoter) (017491, the Jackson Laboratory), *Alb-Cre* [38] (Cre-recombinase under mouse albumin promoter) (003574, the Jackson Laboratory), and *Vil-Cre* [39] (Cre-recombinase under mouse IE-specific villin 1 promoter) (004586, the Jackson Laboratory) transgenic mice, respectively. All the tissue-specific Cre mice had been backcrossed to C57BL/6 for at least 10 generations when purchased from the Jackson Laboratory, thus the resulting tissue-specific CMG2-null mice used in this study harbor LT-resistant Nlrp1 alleles, and are resistant to LT-induced rapid myeloid cell death. Gene-targeted and transgenic mice used in this study are listed in Table 1.

Genotyping was performed by PCR using mouse ear DNA. In analyzing CMG2 expression, total RNA isolated from various mouse tissues using TRIZOL reagent (Invitrogen, Carlsbad, CA) was reverse transcribed using the SuperScript III Reverse Transcriptase (Invitrogen). The 451-bp TM-containing CMG2 cDNA fragment was amplified from WT tissues using a forward and reverse primer pair, as listed in Extended Data Table 1. These primers amplify a 355-bp TM-deleted CMG2 cDNA fragment from CMG2 TM domain deleted tissues. Two biological replicates were performed for reverse transcription (RT)-PCR analyses of tissue-specific deletion of CMG2.

Generation of tissue-specificCMG2 transgenic mice

Mouse full-length CMG2 cDNA was isolated by RT-PCR from mouse bone-marrow derived macrophages and cloned into EcoRI/NheI sites of pCLE vector [24,40], resulting in CMG2 transgenic vector pCLEmCMG2 containing mouse CMG2 cDNA under the control of the CAG promoter (P_{CAG}, a combination of the cytomegalovirus early enhancer element and chicken β-actin promoter). A loxP-stop-loxP cassette (LSL, a DNA fragment containing EGFP coding sequence followed by a poly A terminator [24]) flanked by loxP sites was placed between P_{CAG} and CMG2 cDNA (Extended Data Fig. 2a). After removing the non-relevant part by XhoI and DraIII digestions, the transgenic vector was microinjected into the pronuclei of fertilized eggs to generate transgenic mice (C57BL/6 background). The founder lines were genotyped by Southern blot analyses. Because P_{CAG} is a ubiquitous promoter, the resulting transgenic mice (*LSL-CMG2*) exhibit whole body green fluorescence and thus could be identified with GFP visualization using GFP visualization goggles (Model FHS/F-00, BLS Ltd., Budapest, Hungary). The transgenic mice do not express the CMG2

transgene until bred with cell-type specific *Cre*- transgenic mice to remove the LSL cassette and place P_{CAG} adjacent to the CMG2 cDNA (Extended Data Fig. 2a). Thus, EC-specific CMG2-expressing mice (*CMG2*^{EC}) were obtained by breeding the green *LSL-CMG2* mice with *Cdh-Cre* mice to delete the LSL cassette only in ECs, and by subsequent breeding with whole-body *CMG2*$^{-/-}$ mice to eliminate expression of the endogenous CMG2 gene. CM-, SM/CM-, IE- and hepatocyte-specific CMG2-expressing mice were generated similarly using the corresponding cell-type specific Cre-expressing mice. The PCR primers for genotyping these mice are listed in Extended Data Table 1. CMG2 transgenic mice were generated by SAIC/NCI-FCRDC-Frederick under contract with the National Institute of Allergy and Infectious Diseases.

Animal studies

All animal studies were carried out in accordance with protocols approved by the National Institute of Allergy and Infectious Diseases Animal Care and Use Committee. In LT challenge experiments, 8–10 week old male and female mice with various genotypes were injected with one or two doses of 100 μg LT (100 μg PA plus 100 μg LF) in 0.5 ml PBS intraperitoneally or 50 μg LT in 0.2 ml PBS intravenously. In ET challenge experiments, mice described above were injected 25–50 μg ET in 0.2 ml PBS intravenously or in 0.5 ml PBS intraperitoneally. PA, LF, EF, and FP59 proteins were purified from a non-virulent *B. anthracis* strain as previously described [41–43]. For infection studies, *B. anthracis* spores were prepared from the non-encapsulated, toxigenic *B. anthracis* Sterne-like strain A35 [31] as previously described [32]. Mice were injected with 4×10^8 A35 spores subcutaneously. For vegetative bacterial infections, mice were injected with 2×10^6 A35 bacteria via tail vein. Our previous studies demonstrate that 5–10 mice per treatment group are sufficient for statistical analyses in toxin challenge experiments [4,13,15]. Thus, we use 5–10 or more mice per group to ensure statistical power. At least two biological replicates were performed for each toxin challenge experiment. The mice were grouped based on genotypes. When the mice in same genotype received different treatments, they were randomly assigned to treatment groups. We used the following criteria to score mouse disease progression induced by LT or ET: 0: healthy mouse; 1: slight ruffled coat but no problem in running around cage; 2: ruffled coat and decrease in activity; 3: ruffled coat, hunched posture and little movement; 3.5: moribund; 4: found dead. All toxin-challenged or infected mice were monitored twice daily for 2 weeks post-challenge for signs of malaise or mortality by investigators and animal caretakers who were unaware of genotypes.

For the tissue wet/dry ratio measurements, mice treated with PBS or ET were killed by CO_2 inhalation, and organs collected and weighed. Organs were dried by incubation in an oven at 45°C overnight. For the footpad skin edema model, mice were injected intradermally in one foot pad with 0.25 μg ET in 20 μL PBS. Footpad edema was monitored at 8 and 20 h after injection by measuring dorsal/planar and medial/lateral sizes using digital calipers.

Murine c-Troponin-I ELISA kit (Life Diagnostics, West Chester, PA) was used to measure the cardiac biomarker c-Troponin-I in mouse serum samples according to the manufacturer's protocol. Mice of various genotypes were treated intraperitoneally with 100 μg LT and bled at indicated time points post-challenge for serum c-Troponin-I measurements. For

echocardiography studies, mice were kept under isoflurane anesthesia on a heating pad with body temperature monitoring (by anal probe) throughout the procedure. Baseline left ventricular short and long axis views were obtained with the Vevo 770 system at the NIH Mouse Imaging Facility. All measurements were performed in blinded fashion.

Mouse endothelial cell isolation and cytotoxicity assay

ECs were isolated and cultured as described previously [33]. Briefly, three mouse lungs were digested with type I collagenase and plated on gelatin and collagen-coated flasks. The cells were then subjected to sequential negative sorting by magnetic beads coated with a sheep anti-rat antibody using a Fc Blocker (rat anti-mouse CD16/CD32, Cat. 553142, BD Pharmingen, San Diego, CA) to remove macrophages and positive sorting by magnetic beads using an anti-intermolecular adhesion molecule 2 (ICAM2 or CD102) antibody (Cat. 553326, rat anti-mouse CD102, BD Pharmingen) to isolate ECs (ICAM2 positive cells). The cells other than ECs (non-ECs, ICAM2 negative cells) were also isolated simultaneously as controls. These primary cells were used within 5 passages after isolation. For cytotoxicity assays, ECs, non-ECs, and Chinese hamster ovary (CHO) cells were grown in 96-well plates and treated with serial dilutions of PA or PA-L687A combined with 100 ng/ml FP59 for 48 h. PA-L687A was first described in [44] and found in this study to be a CMG2-preferable PA mutant. FP59 is a fusion protein of LF amino acids 1–254 and the catalytic domain of *Pseudomonas aeruginosa* exotoxin A that kills cells by ADP-ribosylation of eukaryotic elongation factor-2 after delivery to cytosol by PA [22,23]. Cell viabilities were then assayed by MTT (3-[4,5-dimethylthiazol-2-yl]-2,5-diphenyltetrazolium bromide) as described previously [34], expressed as % of MTT signals of untreated cells. The CHO cells that express only TEM8 (PR230(TEM8)) or CMG2 (PR230(CMG2)) were described previously [42].

Histology

Mice treated with PBS, LT (100 μg, intraperitoneally), or ET (50 μg, intravenously) were killed by CO_2 inhalation, and hearts, livers, lungs, kidneys, and spleens collected and fixed in 4% paraformaldehyde for 24 h, embedded in paraffin, sectioned, stained with hematoxylin/eosin and subjected to microscopic analysis.

Statistical analyses

GraphPad Prism 6 was used for statistical analyses. For comparison of mouse survival curves, the Log-rank (Mantel-Cox) test was used. For differences in tissue edema between two groups, the two-tailed unpaired Student's *t* test was used. $P < 0.05$ was considered statistically significant.

Acknowledgments

This research was supported by the intramural research programs of the National Institute of Allergy and Infectious Diseases and the National Heart, Lung, and Blood Institute, National Institutes of Health. We thank Lionel Feigenbaum and the staff at SAIC/NCI Frederick for generation of the founder CMG2 transgenic mice. We thank Ashok Kulkarni and Bradford Hall (National Institute of Dental and Cranial Research, NIH), Brenda Klaunberg and Stasia Anderson (NIH Mouse Imaging Facility), and Inka Sastalla, Clinton Leysath, and Christopher Bachran (Leppla lab) for helpful discussions, and Daryl Despres (NIH Mouse Imaging Facility) for help with echocardiography.

References

1. Moayeri M, Leppla SH. Cellular and systemic effects of anthrax lethal toxin and edema toxin. Mol Aspects Med. 2009; 30:439–455. [PubMed: 19638283]
2. Bradley KA, Mogridge J, Mourez M, Collier RJ, Young JA. Identification of the cellular receptor for anthrax toxin. Nature. 2001; 414:225–229. [PubMed: 11700562]
3. Scobie HM, Rainey GJ, Bradley KA, Young JA. Human capillary morphogenesis protein 2 functions as an anthrax toxin receptor. Proc Natl Acad Sci U S A. 2003; 100:5170–5174. [PubMed: 12700348]
4. Liu S, et al. Capillary morphogenesis protein-2 is the major receptor mediating lethality of anthrax toxin in vivo. Proc Natl Acad Sci U S A. 2009; 106:12424–12429. [PubMed: 19617532]
5. Leppla SH. Anthrax toxin edema factor: a bacterial adenylate cyclase that increases cyclic AMP concentrations of eukaryotic cells. Proc Natl Acad Sci U S A. 1982; 79:3162–3166. [PubMed: 6285339]
6. Firoved AM, et al. Bacillus anthracis edema toxin causes extensive tissue lesions and rapid lethality in mice. Am J Pathol. 2005; 167:1309–1320. [PubMed: 16251415]
7. Duesbery NS, et al. Proteolytic inactivation of MAP-kinase-kinase by anthrax lethal factor. Science. 1998; 280:734–737. [PubMed: 9563949]
8. Vitale G, et al. Anthrax lethal factor cleaves the N-terminus of MAPKKs and induces tyrosine/threonine phosphorylation of MAPKs in cultured macrophages. Biochem Biophys Res Commun. 1998; 248:706–711. [PubMed: 9703991]
9. Vitale G, Bernardi L, Napolitani G, Mock M, Montecucco C. Susceptibility of mitogen-activated protein kinase kinase family members to proteolysis by anthrax lethal factor. Biochem J. 2000; 352(Pt 3):739–745. [PubMed: 11104681]
10. Newman ZL, et al. Susceptibility to anthrax lethal toxin-induced rat death is controlled by a single chromosome 10 locus that includes rNlrp1. PLoS Pathog. 2010; 6:e1000906. [PubMed: 20502689]
11. Levinsohn JL, et al. Anthrax lethal factor cleavage of Nlrp1 is required for activation of the inflammasome. PLoS Pathog. 2012; 8:e1002638. [PubMed: 22479187]
12. Pezard C, Berche P, Mock M. Contribution of individual toxin components to virulence of Bacillus anthracis. Infect Immun. 1991; 59:3472–3477. [PubMed: 1910002]
13. Liu S, et al. Anthrax toxin targeting of myeloid cells through the CMG2 receptor Is essential for establishment of Bacillus anthracis infections in mice. Cell Host Microbe. 2010; 8:455–462. [PubMed: 21075356]
14. Guichard A, Nizet V, Bier E. New insights into the biological effects of anthrax toxins: linking cellular to organismal responses. Microbes Infect. 2012; 5:48–61.
15. Moayeri M, Haines D, Young HA, Leppla SH. Bacillus anthracis lethal toxin induces TNF-independent hypoxia-mediated toxicity in mice. J Clin Invest. 2003; 112:670–682. [PubMed: 12952916]
16. Moayeri M, et al. The heart is an early target of anthrax lethal toxin in mice: a protective role for neuronal nitric oxide synthase (nNOS). PLoS Pathog. 2009; 4:e1000456. [PubMed: 19478875]
17. Bolcome RE III, et al. Anthrax lethal toxin induces cell death-independent permeability in zebrafish vasculature. Proc Natl Acad Sci U S A. 2008; 105:2439–2444. [PubMed: 18268319]
18. Guichard A, et al. Anthrax toxins cooperatively inhibit endocytic recycling by the Rab11/Sec15 exocyst. Nature. 2010; 467:854–858. [PubMed: 20944747]
19. Warfel JM, Steele AD, D'Agnillo F. Anthrax lethal toxin induces endothelial barrier dysfunction. Am JPathol. 2005; 166:1871–1881. [PubMed: 15920171]
20. Maddugoda MP, et al. cAMP signaling by anthrax edema toxin induces transendothelial cell tunnels, which are resealed by MIM via Arp2/3-driven actin polymerization. Cell Host Microbe. 2011; 10:464–474. [PubMed: 22100162]
21. Ghosh CC, et al. Impaired function of the Tie-2 receptor contributes to vascular leakage and lethality in anthrax. Proc Natl Acad Sci U S A. 2012; 109:10024–10029. [PubMed: 22665799]

22. Arora N, Klimpel KR, Singh Y, Leppla SH. Fusions of anthrax toxin lethal factor to the ADP-ribosylation domain of Pseudomonas exotoxin A are potent cytotoxins which are translocated to the cytosol of mammalian cells. J Biol Chem. 1992; 267:15542–15548. [PubMed: 1639793]
23. Liu S, et al. Diphthamide modification on eukaryotic elongation factor 2 is needed to assure fidelity of mRNA translation and mouse development. Proc Natl Acad Sci U S A. 2012; 109:13817–13822. [PubMed: 22869748]
24. Bradley SV, et al. Degenerative phenotypes caused by the combined deficiency of murine HIP1 and HIP1r are rescued by human HIP1. Hum Mol Genet. 2007; 16:1279–1292. [PubMed: 17452370]
25. Lepore JJ, et al. High-efficiency somatic mutagenesis in smooth muscle cells and cardiac myocytes in SM22alpha-Cre transgenic mice. Genesis. 2005; 41:179–184. [PubMed: 15789423]
26. Dal Molin F, et al. Ratio of lethal and edema factors in rabbit systemic anthrax. Toxicon. 2008; 52:824–828. [PubMed: 18812184]
27. Sirard JC, Mock M, Fouet A. The three Bacillus anthracis toxin genes are coordinately regulated by bicarbonate and temperature. J Bacteriol. 1994; 176:5188–5192. [PubMed: 8051039]
28. Mabry R, et al. Detection of anthrax toxin in the serum of animals infected with Bacillus anthracis by using engineered immunoassays. Clin Vaccine Immunol. 2006; 13:671–677. [PubMed: 16760326]
29. Jernigan JA, et al. Bioterrorism-related inhalational anthrax: The first 10 cases reported in the United States. Emerg Infect Dis. 2001; 7:933–944. [PubMed: 11747719]
30. Guarner J, et al. Pathology and pathogenesis of bioterrorism-related inhalational anthrax. Am JPathol. 2003; 163:701–709. [PubMed: 12875989]
31. Pomerantsev AP, Sitaraman R, Galloway CR, Kivovich V, Leppla SH. Genome engineering in Bacillus anthracis using Cre recombinase. Infect Immun. 2006; 74:682–693. [PubMed: 16369025]
32. Hu H, Sa Q, Koehler TM, Aronson AI, Zhou D. Inactivation of Bacillus anthracis spores in murine primary macrophages. Cell Microbiol. 2006; 8:1634–1642. [PubMed: 16984418]
33. Reynolds LE, Hodivala-Dilke KM. Primary mouse endothelial cell culture for assays of angiogenesis. Methods Mol Med. 2006; 120:503–509. [PubMed: 16491622]
34. Liu S, Leppla SH. Cell surface tumor endothelium marker 8 cytoplasmic tail-independent anthrax toxin binding, proteolytic processing, oligomer formation, and internalization. J Biol Chem. 2003; 278:5227–5234. [PubMed: 12468536]
35. Alva JA, et al. VE-Cadherin-Cre-recombinase transgenic mouse: a tool for lineage analysis and gene deletion in endothelial cells. Dev Dyn. 2006; 235:759–767. [PubMed: 16450386]
36. Agah R, et al. Gene recombination in postmitotic cells. Targeted expression of Cre recombinase provokes cardiac-restricted, site-specific rearrangement in adult ventricular muscle in vivo. J Clin Invest. 1997; 100:169–179. [PubMed: 9202069]
37. Holtwick R, et al. Smooth muscle-selective deletion of guanylyl cyclase-A prevents the acute but not chronic effects of ANP on blood pressure. Proc Natl Acad Sci U S A. 2002; 99:7142–7147. [PubMed: 11997476]
38. Postic C, et al. Dual roles for glucokinase in glucose homeostasis as determined by liver and pancreatic beta cell-specific gene knock-outs using Cre recombinase. J Biol Chem. 1999; 274:305–315. [PubMed: 9867845]
39. Braunstein EM, et al. Villin: A marker for development of the epithelial pyloric border. Dev Dyn. 2002; 224:90–102. [PubMed: 11984877]
40. Hall BE, et al. Conditional overexpression of TGF-beta1 disrupts mouse salivary gland development and function. Lab Invest. 2010; 90:543–555. [PubMed: 20142803]
41. Pomerantsev AP, et al. A Bacillus anthracis strain deleted for six proteases serves as an effective host for production of recombinant proteins. Protein Expr Purif. 2011; 80:80–90. [PubMed: 21827967]
42. Liu S, Leung HJ, Leppla SH. Characterization of the interaction between anthrax toxin and its cellular receptors. Cell Microbiol. 2007; 9:977–987. [PubMed: 17381430]
43. Gupta PK, Moayeri M, Crown D, Fattah RJ, Leppla SH. Role of N-terminal amino acids in the potency of anthrax lethal factor. PLoS One. 2008; 3:e3130. [PubMed: 18769623]

44. Rosovitz MJ, et al. Alanine scanning mutations in domain 4 of anthrax toxin protective antigen reveal residues important for binding to the cellular receptor and to a neutralizing monoclonal antibody. J Biol Chem. 2003; 278:30936–30944. [PubMed: 12771151]

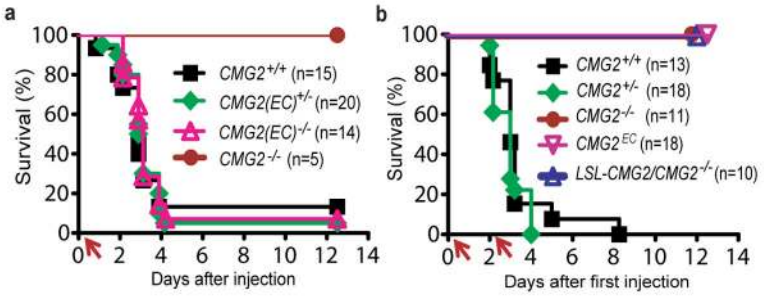

Figure 1. LT targeting of endothelial cells is not lethal to mice

a, b, Susceptibility of *CMG2(EC)*$^{-/-}$ (**a**) and *CMG2*^{EC} mice (**b**) to LT. Mice were treated intraperitoneally with single (**a**) or two doses (**b**) (arrows) of 100 μg LT (100 μg PA + 100 μg LF), and monitored for survival.

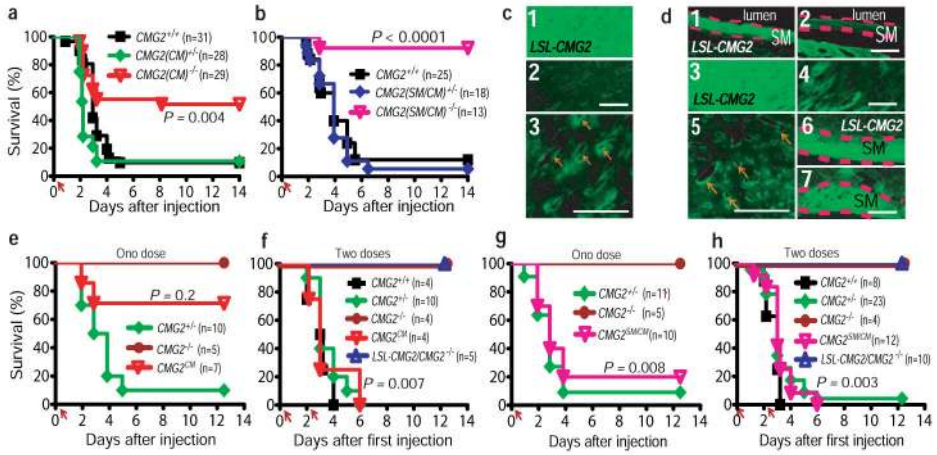

Figure 2. Targeting of cardiomyocytes and smooth muscle cells by LT is sufficient for lethality

a, b, Increased resistance of CM- and SM-specific CMG2-null mice to LT. *CMG2(CM)*$^{-/-}$ (**a**), *CMG2(SM/CM)*$^{-/-}$ (**b**), and their littermate controls were challenged intraperitoneally with 100 μg LT. *CMG2(CM)*$^{-/-}$ vs. *CMG2*$^{+/+}$ mice, $P = 0.004$; *CMG2(SM/CM)*$^{-/-}$ vs. *CMG2*$^{+/+}$ mice, $P < 0.0001$. Log-rank test.

c, Selective activation of CMG2 transgene in CMs of *CMG2*^{CM} mice. Representative fluorescence microscopy of heart from *LSL-CMG2* mice (**1**) (n = 2) and *CMG2*^{CM} mice (**2, 3**) (n = 2). Selective loss of GFP expression in CMs (**2** and **3** compared to **1**) but not ECs (arrows in **3**) is shown. Scale bar, 100 μm.

d, Selective activation of CMG2 transgene in SMs and CMs from *CMG2*$^{SM/CM}$ mice. Representative fluorescence microscopy of aorta (**2**), heart (**4** and **5**), small intestine (smooth muscle) (**7**) from *CMG2*$^{SM/CM}$ mice (n = 3), and aorta (**1**), heart (**3**), small intestine (**6**) from *LSL*-CMG2 mice (n = 2). Selective loss of GFP expression in vascular SMs (in aorta) and CMs (**2**, **4**, and **5** compared to **1** and **3**) but not SMs in small intestine (**7** compared to **6**) and not ECs in heart (arrows in 5) is shown. Scale bar, 100 μm.

e–h, Sensitivity of *CMG2*^{CM} mice (**e**, **f**) and *CMG2*$^{SM/CM}$ mice (**g**, **h**) to single (**e, g**) or 2 doses (**f, h**) of 100 μg LT (intraperitoneally). *CMG2*^{CM} vs. *CMG2*$^{-/-}$ mice, $P = 0.2$ in (**e**); $P = 0.007$ in (**f**). *CMG2*$^{SM/CM}$ vs. *CMG2*$^{-/-}$ mice $P = 0.008$ in (**g**); $P = 0.003$ in (**h**). Log-rank test.

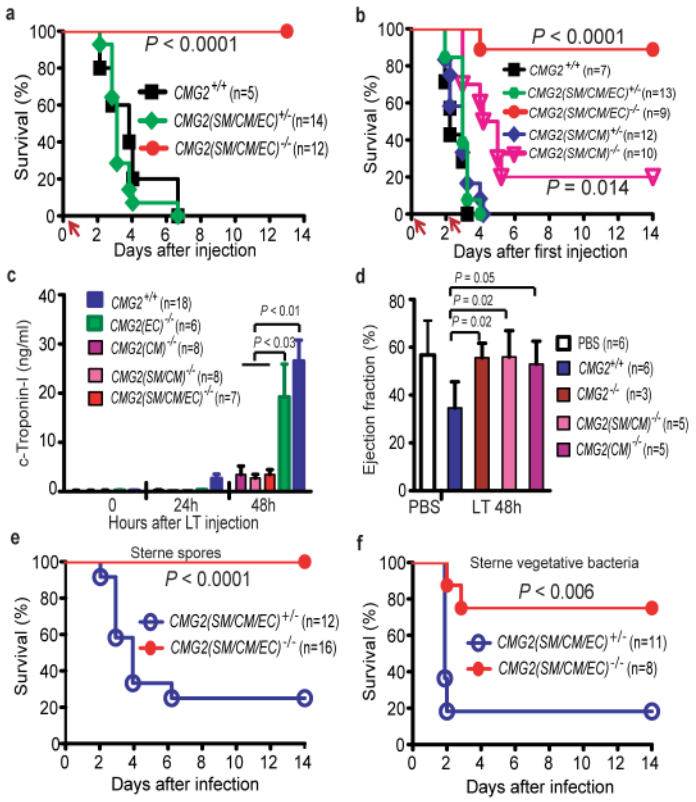

Figure 3. Mice lacking CMG2 receptor in the three major cell types of the cardiovascular system are highly resistant to LT and B. anthracis infection

a, b, Resistance of *CMG2(SM/CM/EC)*$^{-/-}$ mice to challenge with one (**a**) or two doses (**b**) of 100 μg LT (intraperitoneally). In **a**, *CMG2(SM/CM/EC)*$^{-/-}$ vs. *CMG2*$^{+/+}$ mice, $P < 0.0001$. In **b**, *CMG2(SM/CM/EC)*$^{-/-}$ vs. *CMG2*$^{+/+}$ mice, $P < 0.0001$; *CMG2(SM/CM)*$^{-/-}$ vs. *CMG2*$^{+/+}$ m ce, $P = 0.014$. Log-rank test.

c, Serum levels of cardiac biomarker c-Troponin-I in mice treated intraperitoneally with 100 μg LT. Error bars, S.E. Two-tailed unpaired *t*-test.

d, Echocardiography analyses of mice challenged intraperitoneally with 100 μg LT. Error bars, S.D. Two-tailed unpaired *t*-test.

e, **f**, Resistance of the *CMG2(SM/CM/EC)*$^{-/-}$ mice to *B. anthracis* infection with 4×10^8 Sterne spores (**e**) or 2×10^6 vegetative bacteria (**f**). Log-rank test.

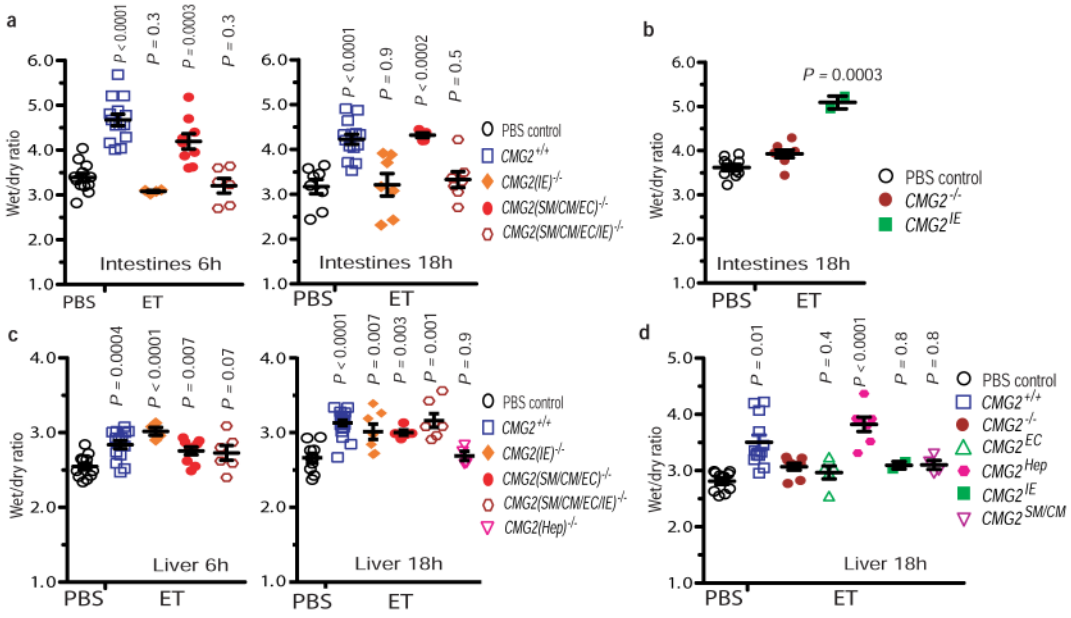

Figure 4. ET directly targets intestinal epithelial cells and hepatocytes

a–d, Wet/dry ratios of intestines (**a**, **b**) or livers (**c**, **d**) of the cell-type-specific CMG2-null mice (**a,c**), and the cell-type-specific CMG2-expressing mice (**b, d**) after ET challenge (30 μg, intravenously). Because PBS treated WT and mutant mice have a similar baseline of wet/dry ratio, the PBS control groups were pooled for each tissue. In **a** and **c**, the *P* values of the indicated groups vs. PBS controls are given. In **b** and **d**, the *P* values of the indicated groups vs. *CMG2*$^{-/-}$ group are given. Error bars, S.E. Two-tailed unpaired *t*-test.

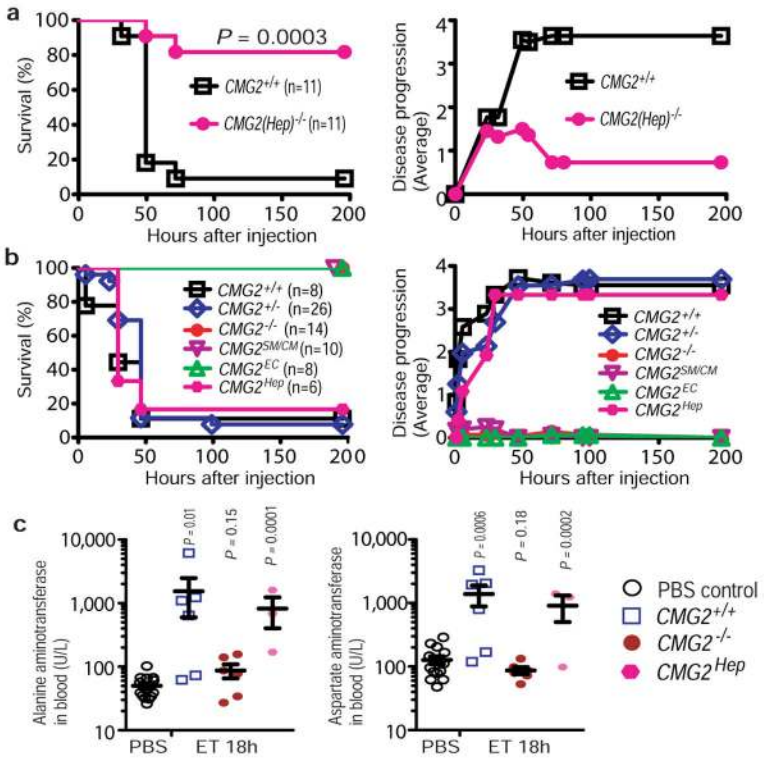

Figure 5. epatocytes are amajor target of ET-induced lethality

a, Survival of *CMG2(Hep)*$^{-/-}$ mice following ET (35 μg, intravenously) challenge. Right panel shows the disease progression of the challenged mice. Please see Methods for disease progression scoring criteria. Log-rank test.

b, Sensitivity of *CMG2*^{Hep} mice to ET. The cell-type-specific CMG2-expressing mice and their respective littermate controls were challenged with ET (50 μg, intravenously). *CMG2*^{Hep} vs. *CMG2*$^{-/-}$ mice, $P = 0.003$. Log-rank test.

c, Serum levels of alanine aminotransferase and aspartate aminotransferase in ET-challenged mice (30 μg, intravenously). Error bars, S.E. Two-tailed unpaired *t*-test.

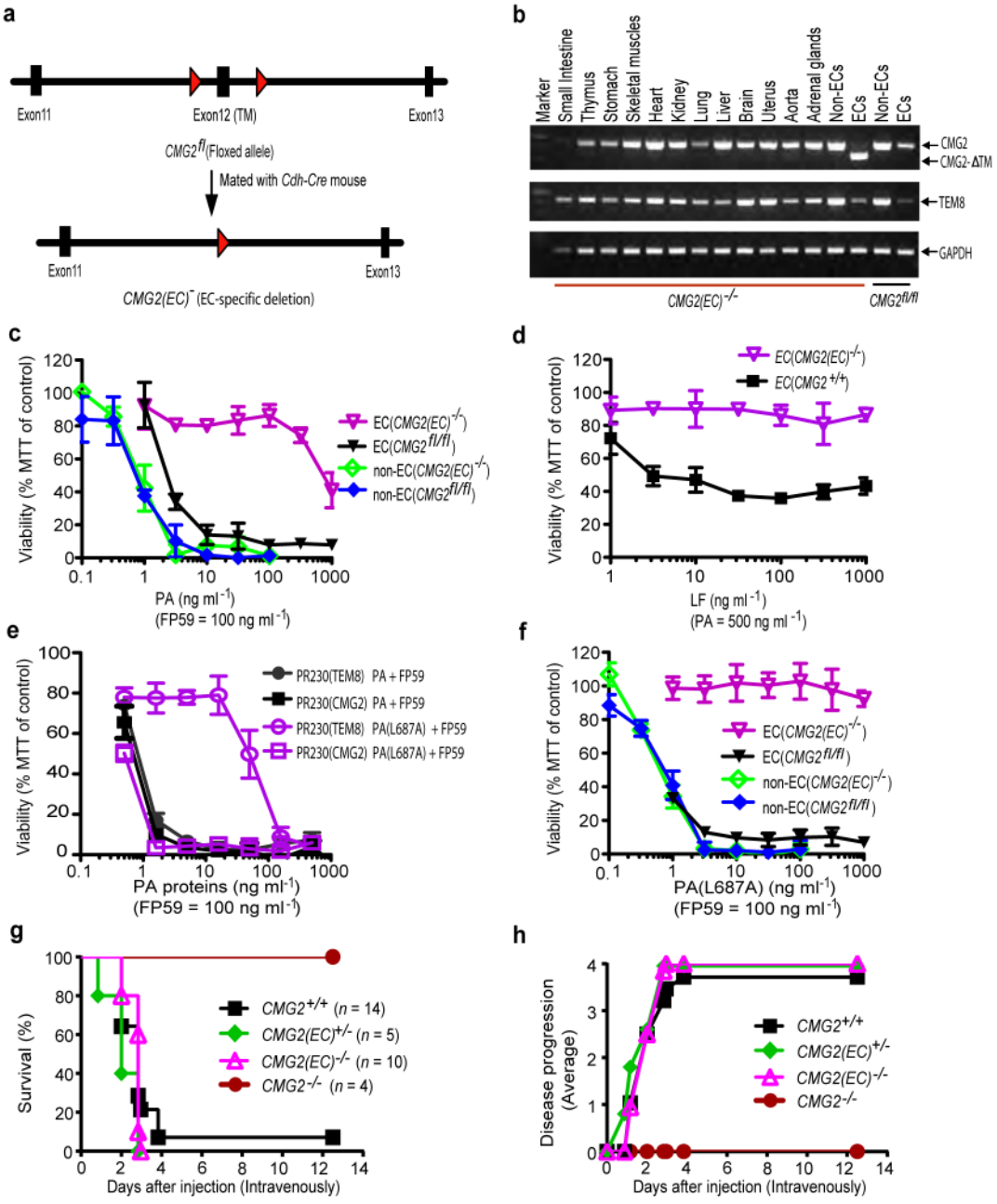

Extended Data Figure 1. Generation of endothelial-cell-specific CMG2-null mice

a, Strategy for generation of EC-specific CMG2-null mice. Diagram shows *CMG2*^{f} allele having exon 12 (encoding transmembrane domain, TM) flanked by loxP sites and the EC-specific CMG2-null allele (*CMG2(EC)*$^{-}$). The red arrowheads indicate loxP sites. The homozygous EC-specific CMG2-null mice (*CMG2(EC)*$^{-/-}$) were obtained by intercrossing of *CMG2(EC)*$^{+/-}$ mice. Other cell-type specific CMG2-null mice were made similarly by using the corresponding cell-type specific Cre transgenic mice.

b, RT-PCR analyses of CMG2 TM domain deletion in various tissues of *CMG2(EC)*$^{-/-}$ mice. Primers flanking the CMG2 TM were used to amplify a CMG2 cDNA fragment. ECs

and non-ECs were isolated simultaneously from lungs pooled from three *CMG2(EC)*$^{-/-}$ mice and three *CMG2*$^{f/f}$ control mice. Representative of two independent experiments is shown. Expression of TEM8 and GAPDH in these samples is also shown.

c, Sensitivity of ECs and non-ECs from *CMG2*$^{f/f}$ and *CMG2(EC)*$^{-/-}$ mice to PA + FP59. Cells were treated with various concentrations of PA and FP59 (100 ng/ml) for 48 h. Cell viability was evaluated by MTT assay, expressed as relative MTT signals to untreated cells. Error bars, S.D.

d, Resistance of ECs from *CMG2(EC)*$^{-/-}$ mice to LT. ECs from *CMG2(EC)*$^{-/-}$ and WT mice were treated with various concentrations of LF and PA (500 ng/ml) for 48 h.

e, PA-L687A preferentially kills CMG2-expressing cells. Cells were treated with various concentrations of PA or PA-L687A and 100 ng/ml FP59 for 48 h. PR230(TEM8) and PR230(CMG2) are engineered CHO cells express only TEM8 or CMG2. Note, PR230(TEM8) cells are 100-fold more resistant than PR230(CMG2) cells to PA-L687A + FP59.

f, Sensitivity of ECs and non-ECs from *CMG2*$^{f/f}$ and *CMG2(EC)*$^{-/-}$ mice to PA-L687A + FP59. Cells were incubated for 48 h with various concentrations of PA-L687A and 100 ng/ml FP59. Error bars, S.D.

g, Susceptibility of *CMG2(EC)*$^{-/-}$ mice to LT. *CMG2(EC)*$^{-/-}$ mice and their littermate controls were injected intravenously with 50 μg LT (50 μg PA + 50 μg LF), and monitored for survival. Whole-body *CMG2*$^{-/-}$ mice were included as additional controls.

h, Disease progression of the LT-challenged mice in panel **g**. Please see Methods for disease progression scoring criteria.

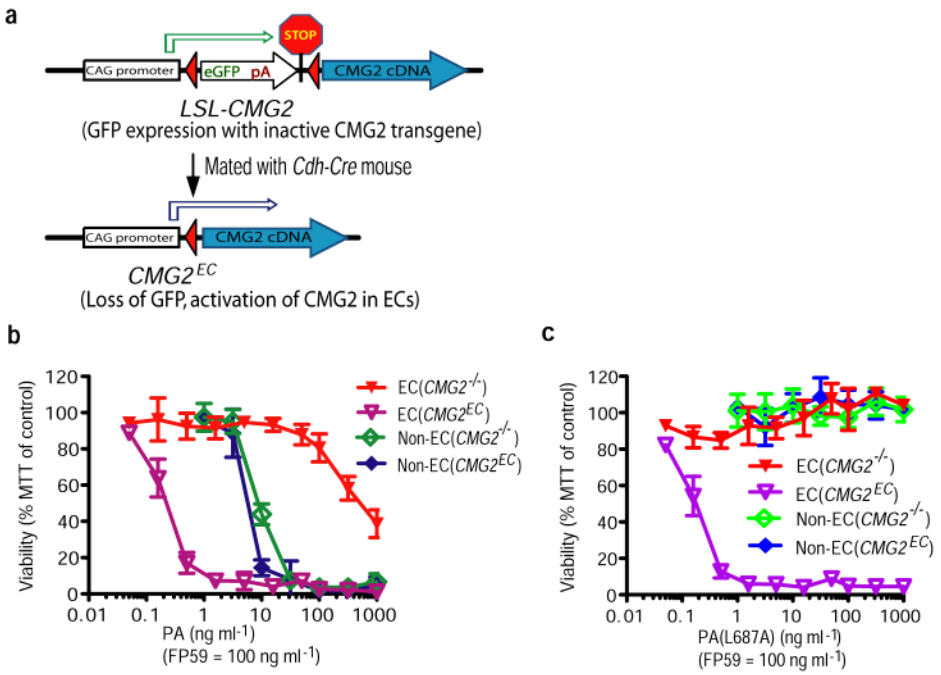

Extended Data Figure 2. Generation of endothelial-cell-specific CMG2-expressing mice

a Strategy for generation of EC-specific CMG2-expressing mice. In the CMG2 transgenic vector (LSL-CMG2), a loxP-stop-loxP cassette containing a promoterless EGFP and a polyA stop signal flanked by loxP sites was placed between the CAG promoter and CMG2 cDNA. Activation of CMG2 transgene in ECs ($CMG2^{EC}$) was achieved by breeding *LSL-CMG2* mice with *Cdh-Cre* mice to specifically remove the loxP-stop-loxP cassette in ECs. Other cell-type specific CMG2-expressing mice were made similarly by using the corresponding cell-type specific Cre transgenic mice.

b, c, Regained toxin sensitivity of ECs from $CMG2^{EC}$ mice. ECs and non-ECs from $CMG2^{EC}$ and whole-body $CMG2^{-/-}$ mice were incubated for 48 h with various concentrations of PA (**b**) or PA-L687A (**c**) and 100 ng/ml FP59. Error bars, S.D.

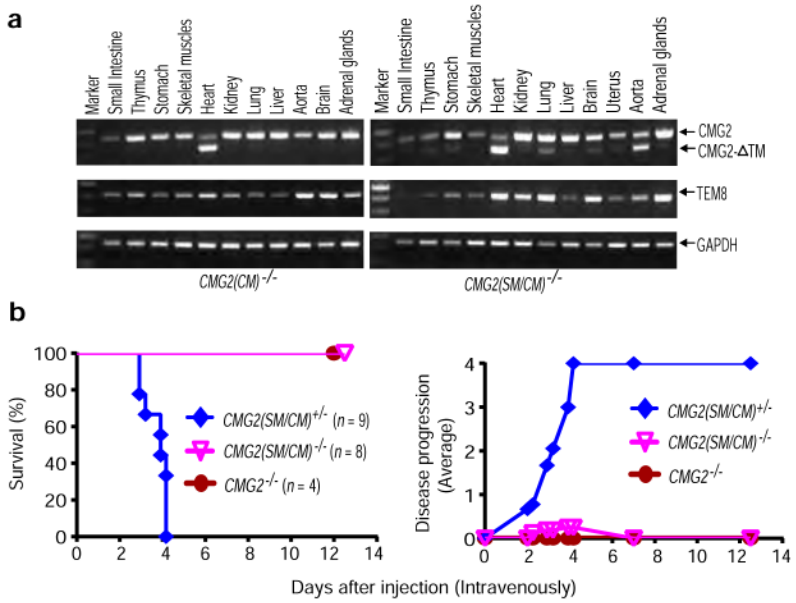

Extended Data Figure 3. Tissue-specific deletion of CMG2 in *CMG2(CM)*$^{-/-}$ and *CMG2(SM/CM)*$^{-/-}$ mice

a, RT-PCR analyses of CMG2 deletion in tissues of *CMG2(CM)*$^{-/-}$ and *CMG2(SM/CM)*$^{-/-}$ mice. CMG2 deletion was detected in heart of *CMG2(CM)*$^{-/-}$ mice and in heart and aorta of *CMG2(SM/CM)*$^{-/-}$ mice. The small fraction of CMG2 deletion that occurred in other tissues of the *CMG2(SM/CM)*$^{-/-}$ mice was due to the existence of varying amounts of vascular smooth muscle cells in those tissues. Representative of two independent experiments is shown.

b, Resistance of SM/CM-specific CMG2-null mice to LT. *CMG2(SM/CM)*$^{-/-}$ mice and their littermate *CMG2(SM/CM)*$^{+/-}$ controls were injected intravenously with 50 μg LT, and monitored for survival. Whole-body *CMG2*$^{-/-}$ mice were included as additional controls. Right panel shows the disease progression of the challenged mice. *CMG2(SM/CM)*$^{-/-}$ vs. *CMG2*$^{+/+}$ mice, $P = 0.0002$. Log-rank test.

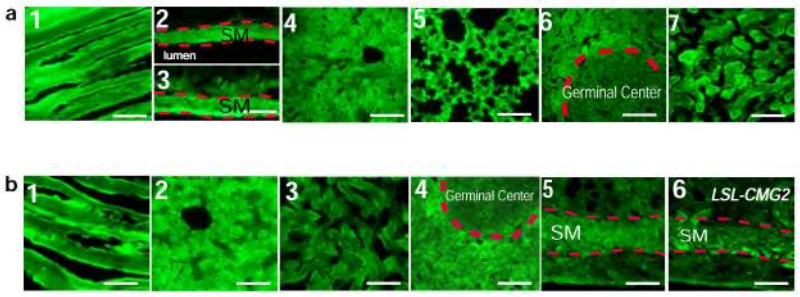

Extended Data Figure 4. Fluorescence microscopic analyses of GFP expression in mouse tissues

a, Representative fluorescence microscopy of skeletal muscle (**1**), aorta (vascular smooth muscle) (**2**), small intestine (smooth muscle) (**3**), liver (**4**), lung (**5**), spleen (**6**), and kidney (cortex) (**7**) from *CMG2*^{CM} mice (n = 2). Scale bar, 100 μm.

b, Representative fluorescence microscopy of skeletal muscle (**1**), liver (**2**), kidney (cortex) (**3**), spleen (**4**), and uterus (**5**) from *CMG2*$^{SM/CM}$ mice (n = 3), and uterus (**6**) from *LSL-CMG2* mice (n = 2). Scale bar, 100 μm.

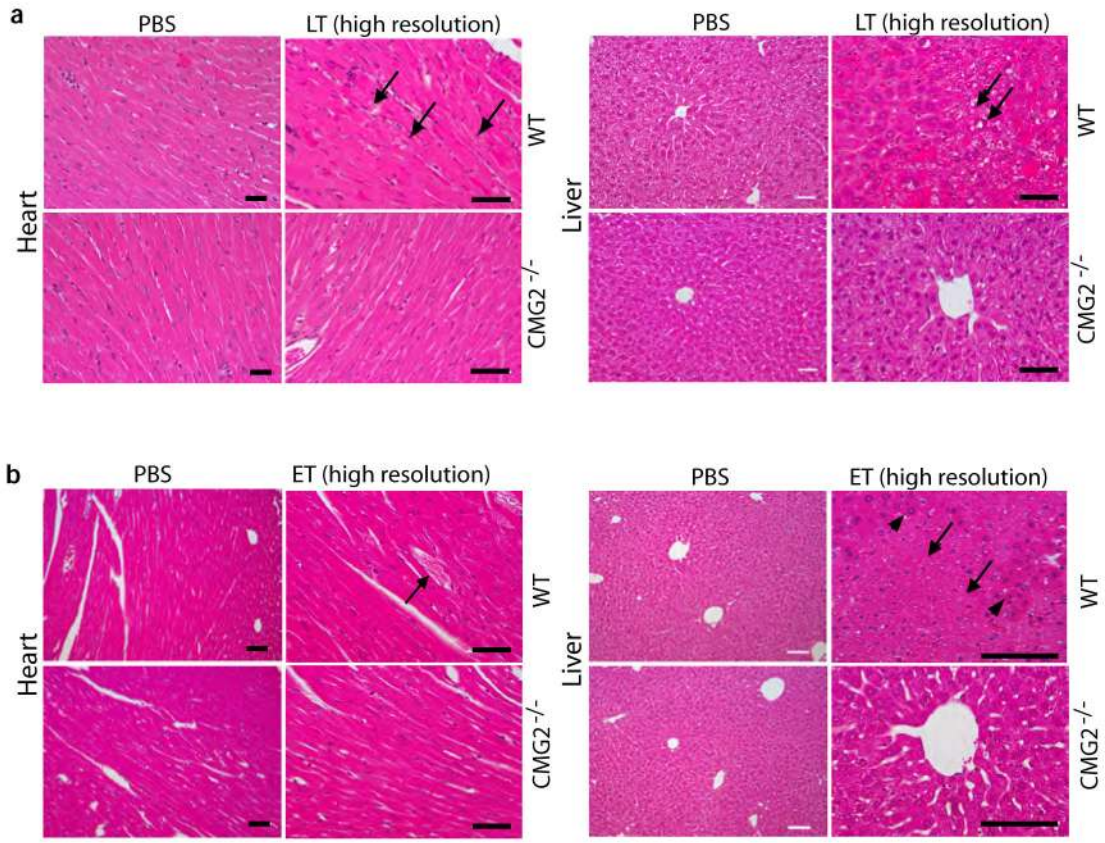

Extended Data Figure 5. Histology of heart and liver of LT and ET-treated mice

a, H&E staining of heart and liver from WT (n = 3) and *CMG2*$^{-/-}$ (n = 3) mice challenged intraperitoneally with 100 μg LT for 48 h. In heart, regions with cardiomyocyte degeneration were found in LT-treated WT but not *CMG2*$^{-/-}$ mice. Arrows show examples of degenerated cardiomyocytes. In liver, regions with mild to modest hepatocyte degeneration were identified in LT-treated WT but not *CMG2*$^{-/-}$ mice. Arrows show examples of degenerated hepatocytes with cytosol vacuolization changes. Scale bar, 50 μm.

b, H&E staining of heart and liver from WT (n = 4) and *CMG2*$^{-/-}$ (n = 3) mice 18 h after 50 μg ET injection (intravenously). In liver, regions with hepatocyte necrotic changes were identified in ET-treated WT mice but not *CMG2*$^{-/-}$ mice. Arrows show necrotic regions, arrow heads indicate examples of intact hepatocytes remained in the necrotic regions. In heart, only scattered degenerated cardiomyocytes (arrow) were found in ET-treated WT but not *CMG2*$^{-/-}$ mice. Scale bar, 50 μm.

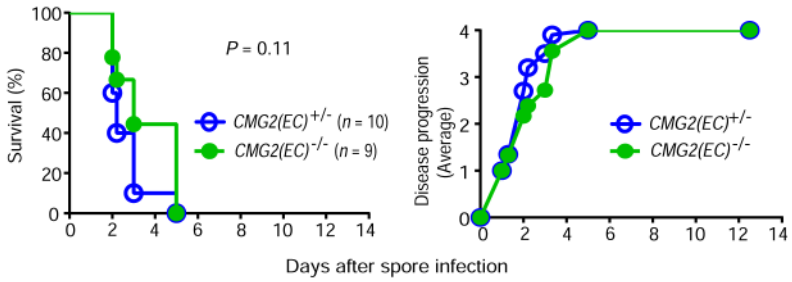

Extended Data Figure 6. Endothelial-cell-specific CMG2-null mice are sensitive to *B. anthracis* infection

CMG2(EC)$^{-/-}$ mice and their littermate heterozygous mice were subcutaneously infected with 4×10^8 Sterne spores and monitored for survival. Right panel shows the disease progression of the challenged mice. Log-rank test.

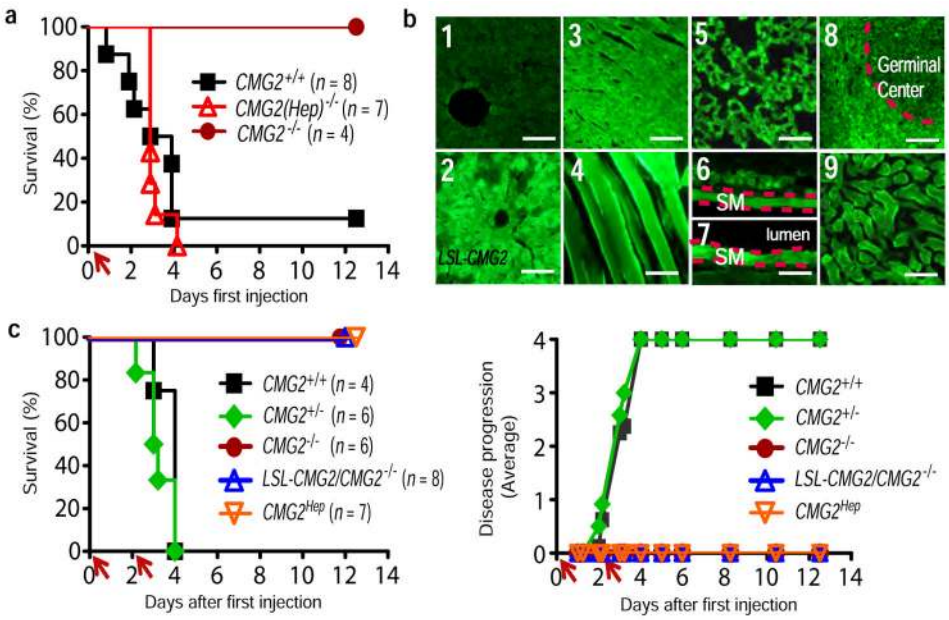

Extended Data Figure 7. LT targeting of liver does not contribute to lethality

a, Susceptibility of the hepatocyte-specific CMG2-null mice to LT. *CMG2(Hep)*$^{-/-}$ mice and their littermate *CMG2*$^{+/+}$ control mice were challenged intraperitoneally with 100 μg LT and monitored for survival. Whole-body *CMG2*$^{-/-}$ mice were included as additional controls.

b, Selective activation of CMG2 transgene in liver of *CMG2*^{Hep} mice. Representative fluorescence microscopy of the liver (**1**), heart (**3**), skeletal muscles (**4**), lung (**5**), small intestines (smooth muscle) (**6**), aorta (**7**), spleen (**8**), and kidney (cortex) (**9**) from *CMG2*^{Hep} mice (n = 2), and liver (**2**) from *LSL-CMG2* mice (n = 2). Selective loss of GFP expression in liver from *CMG2*^{Hep} mice but not *LSL-CMG2* mice (**1** and **2**) is shown. Scale bar, 100 μm.

c, Susceptibility of the hepatocyte-specific CMG2-expressing mice to LT. *CMG2*^{Hep} mice and various control mice as indicated were intraperitoneally challenged with two doses of 100 μg LT and monitored for survival or signs of malaise. Right panel, disease progression of the challenged mice.

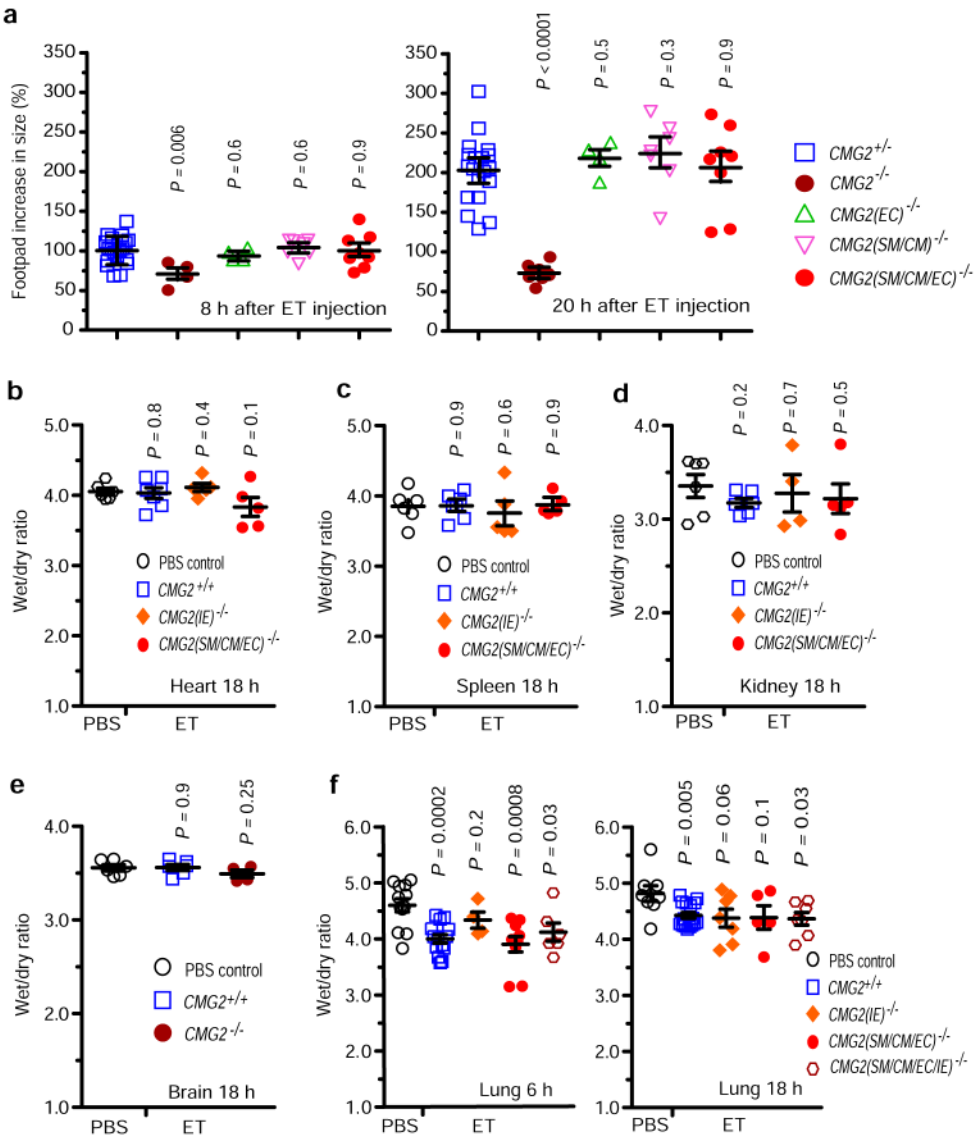

Extended Data Figure 8. Edema in ET-treated mice

a, ET-induced footpad skin edema in mice. Mice with various genotypes were injected with 0.25 μg ET (in 20 μl PBS) and the thicknesses of footpads were measured at 0, 8, and 20 h after injection. ET only induced modest edema in $CMG2^{-/-}$ mice, but caused much higher levels of edema in $CMG2^{+/-}$, $CMG2(EC)^{-/-}$, $CMG2(SM/CM)^{-/-}$, and $CMG2(SM/CM/EC)^{-/-}$ mice. The *P* values of the indicated groups vs. $CMG2^{+/-}$ control group are shown. Each symbol represents one mouse.

b–f, ET does not cause edema in heart, spleen, kidney, lung, and brain. Mice were challenged intravenously with 30 μg ET or PBS, and hearts (**b**), spleens (**c**), kidneys (**d**), brains (**e**), and lungs (**f**) were collected at 6 h or 18 h for tissue wet/dry ratio measurements. The *P* values of the indicated groups vs. the PBS control group are shown. No significant differences are detected among the groups in **b**–**e**. In **f**, decreases in wet/dry ratio of lungs (dehydration) from ET-treated mice were observed. Each symbol represents one mouse. In **a–e**, error bars, S.E; two-tailed unpaired *t*-test.

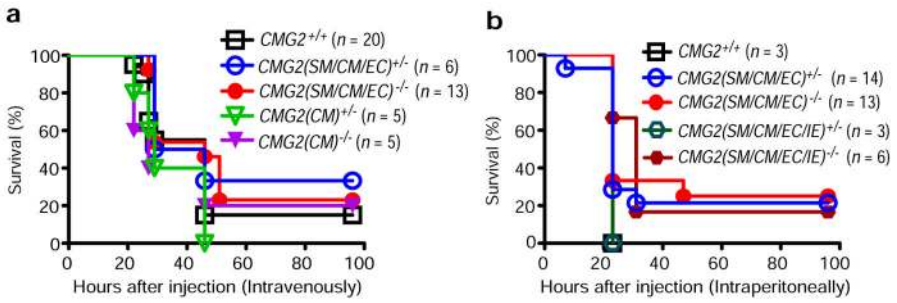

Extended Data Figure 9. Mice with CMG2 deletion in cardiovascular system and intestines remain sensitive to ET

a, **b,** Sensitivity of *CMG2(CM)*$^{-/-}$, *CMG2(SM/CM/EC)*$^{-/-}$, *CMG2(SM/CM/EC/IE)*$^{-/-}$, and their littermate control mice to ET. Mice were challenged intravenously with 25 μg ET (**a**) or intraperitoneally with 50 μg ET (**b**) and survival monitored post-challenge.

Table 1

Nomenclature of gene-targeted and transgenic mice

Mouse description	Genotype	Nomenclature in this study
Whole-body CMG2-null	*CMG2*$^{-/-}$	*CMG2*$^{-/-}$
CMG2 floxed	*CMG2*$^{f/f}$	*CMG2*$^{f/f}$
EC-specific CMG2-null	*CMG2*$^{f/f}$*/Cdh-Cre*	*CMG2(EC)*$^{-/-}$
CM-specific CMG2-null	*CMG2*$^{f/f}$*/Myh6-Cre*	*CMG2(CM)*$^{-/-}$
SM/CM-specific CMG2-null	*CMG2*$^{f/f}$*/SM22-Cre*	*CMG2(SM/CM)*$^{-/-}$
Hep-specific CMG2-null	*CMG2*$^{f/f}$*/Alb-Cre*	*CMG2(Hep)*$^{-/-}$
EC/SM/CM-specific CMG2-null	*CMG2*$^{f/f}$*/SM22-Cre/Cdh-Cre*	*CMG2(SM/CM/EC)*$^{-/-}$
EC/SM/CM/IE-specific CMG2- null	*CMG2*$^{f/f}$*/SM22-Cre/Cdh-Cre/Vil-Cre*	*CMG2(SM/CM/EC/IE)*$^{-/-}$
CMG2 transgenic, inactive	P_{CAG}*-loxPstoploxP-CMG2*	*LSL-CMG2*
Inactive CMG2 transgene in whole-body CMG2-null	P_{CAG}*-loxPstoploxP-CMG2/CMG2*$^{-/-}$	*LSL-CMG2/CMG2*$^{-/-}$
EC-specific CMG2-expressing	P_{CAG}*-loxPstoploxP-CMG2/Cdh-Cre/CMG2*$^{-/-}$	*CMG2*^{EC}
CM-specific CMG2-expressing	P_{CAG}*-loxPstoploxP-CMG2/Myh6-Cre/CMG2*$^{-/-}$	*CMG2*^{CM}
SM/CM-specific CMG2- expressing	P_{CAG}*-loxPstoploxP-CMG2/SM22-Cre/Myh6- Cre/CMG2*$^{-/-}$	*CMG2*$^{SM/CM}$
Hep-specific CMG2-expressing	P_{CAG}*-loxPstoploxP-CMG2/Alb-Cre/CMG2*$^{-/-}$	*CMG2*^{Hep}
IE-specific CMG2-expressing	P_{CAG}*-loxPstoploxP-CMG2/Vil-Cre/CMG2*$^{-/-}$	*CMG2*^{IE}
EC-specific Cre transgenic	*Cdh-Cre*	*Cdh-Cre*
CM-specific Cre transgenic	*Myh6-Cre*	*Myh6-Cre*
SM/CM-specific Cre transgenic	*SM22-Cre*	*SM22-Cre*
Hepe-specific Cre transgenic	*Alb-Cre*	*Alb-Cre*
IE-specific Cre transgenic	*Vil-Cre*	*Vil-Cre*

CM, cardiomyocytes; EC, endothelial cells; Hep, hepatocytes; IE, intestine epithelial cells; loxPstoploxP (LSL), loxP-stop-loxP cassette; PCAG, CAG promoter; SM, vascular smooth muscle cells.

Extended Data Table 1

Primers used for PCR genotyping and cloning

Use		Primer sequence	Size of PCR product (bp)
CMG2 genotyping	Forward1	5′GACTCTTAGGAAGGGTTCCTACTGG3′	WT=350 KO=500 Floxed=550
	Forward2	5′CCAATTTGGAGCTCAGGTTGGTGGA3′	
	Reverse	5′TGTAAGTCATATGGGTAGTGACCTAT3	
General Cre genotyping	Forward	5′ATGTCCAATTTACTGACCGTACACC3′	600
	Reverse	5′CACCGTCAGTACGTGAGATATC3′	
Cdh-Cre genotyping	Forward	5′CTAGAATTGAGGTATGAGTTGAATACC3′	700
	Reverse	5′CACCGTCAGTACGTGAGATATC3′	
Myh6-Cre genotyping	Forward	5′ATGACAGACAGATCCCTCCTATCTCC3′	300
	Reverse	5′CTCATCACTCGTTGCATCATCGAC3′	
SM22-Cre genotyping	Forward	5′TGGTGAGCCAAGCAGACTTCCATGG3′	650
	Reverse	5′CACCGTCAGTACGTGAGATATC3′	
mCMG2 cDNA cloning	Forward	5′AAAAGAATTCGCCACCATGGTGGCCGGTCGGTCCCGGGCGCGCAGCCC TGGGAGCT3′	
	Reverse	5′AAAAGCTAGCTTAATTAATTATTGATGTGGAACCCGGGAGAAGTTTATGC3′	
CMG2 expression	Forward	5′GGAAGAGCAGTCACGTCGATCAGTCA3′	WT=451 KO=355
	Reverse	5′GACCTCCGTAGTAGGAAGCGT3′	
TEM8 expression	Forward	5′TGGCATGAAAGCTGCACTGCAGGTCAGCAT3′	410
	Reverse	5′CATATTCTTGCTCTGGCATCTTGACTCGTG3′	